

Ing. Pavel KOPECKÝ, Ph.D.
Ing. Kamil STANĚK, Ph.D.

CTU in Prague, University Centre
for Energy Efficient Buildings

Review of Three White-Box Lumped Parameter Building Thermal Models

Přezkoumání tří dynamických tepelných modelů budov se sdruženými parametry

Reviewer
Ing. Jiří Cigler, Ph.D.

This paper deals with simplified lumped parameter thermal models of a building. Lumped parameter building thermal models break down building components into a small number of temperature-uniform parts and can be graphically depicted in resistance-capacitance (RC) thermal circuits. The number of unknown variables is extensively reduced which, as a result, considerably increases the speed of the calculation. First, three principal lumped parameter building thermal models are described. Simplifying assumptions on the lumped parameter models are commented on. Then, a simple method for estimating the input parameters from the available information about the buildings is proposed. Finally, comparison with the measured data is reported.

Keywords: building simulation, heat transfer, lumped parameter models, electrical analogy, RC model

Tento článek se zabývá zjednodušenými dynamickými tepelnými modely budovy se sdruženými parametry. Tyto modely rozdělují stavební prvky do velmi malého počtu teplotních uzlů a mohou být graficky zobrazeny tepelnými obvody (elektrická analogie). Nejprve jsou popsány tři základní modely včetně komentáře zjednodušujících předpokladů. Poté je popsána jednoduchá metoda odhadu vstupních parametrů využívající běžně dostupné informace o budově. Nakonec je uvedeno porovnání výsledků jednotlivých modelů s naměřenými daty z experimentu se dvěma identickými neobývanými rodinnými domy.

Klíčová slova: simulace budov, přenos tepla, modely se sdruženými parametry, elektrická analogie, RC model

INTRODUCTION

Lumped parameter building thermal models break down building components into a small number of temperature-uniform parts. Lumped parameter thermal models can be understood as simplified resistance-capacitance (RC) thermal circuits reduced from complex thermal building models. RC thermal circuits have been used for various purposes already. Some examples are listed hereafter.

Nielsen (2005) used a simple lumped parameter model to develop a building design tool. Kämpf et al. (2007) developed a model which was used for the calculations of a building's heat demand on the district level. Huijbregts et al. (2012) used a lumped parameter hygro-thermal building model to study the impact of global warming scenarios on museum buildings. Reynders et al. (2013) used a lumped parameter building model to investigate an intelligent control strategy used to activate structural thermal mass in a single-family house equipped with a heat pump and photovoltaics. Prívará et al. (2011) used a simple lumped parameter room model to implement an advanced predictive controller of a heating system in a real building.

Only a few literature references report the validation of lumped parameter models. Mathews et al. (1994) reported the validation study of a first order model based on the measured data from 32 buildings. Kramer (2012) compared predictions from several lumped parameter models with measured data. Kopecký (2016) used a methodology of BESTEST, see Judkoff and Neymark (1995), to verify three simplified lumped parameter thermal models described in this paper hereafter.

The model predictive control of heating or cooling systems is one of the important practical applications of lumped parameter thermal models. The major challenge of model predictive control is to formulate an accurate and fast model of a building's thermal balance. System identification methods are often utilised for the identification of a suitable model. The measured data, however, does not exist in newly built buildings and buildings in the design stage. The ability to propose model equations

prior to identification experiments is, therefore, essential. The ability to estimate input parameters in model equations (i.e., a reasonable interval of physically acceptable values) in a forward manner from the available information about the building (i.e., drawings, material properties, composition of the building components) is important as well.

The main objective of the paper is to review three existing principal lumped parameter building thermal models. The simplifying assumptions incorporated in the lumped models will be elaborated upon in detail and commented on. A simple white-box method for estimating the input parameters will be proposed. Finally, comparison with the measured data will be reported.

LUMPED PARAMETER BUILDING THERMAL MODELS

RC thermal circuits

Building components

RC thermal circuits of three selected lumped parameter building thermal models are depicted in Figure 1, Figure 2 and Figure 3. They could represent a room, a thermal zone, and even an entire building. Lumped parameter

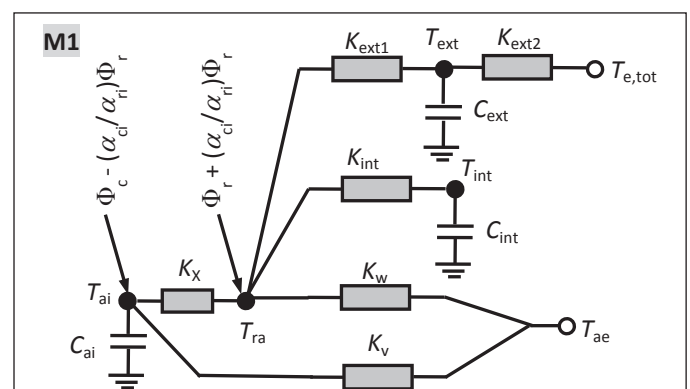


Fig. 1 The RC thermal circuit of model M1

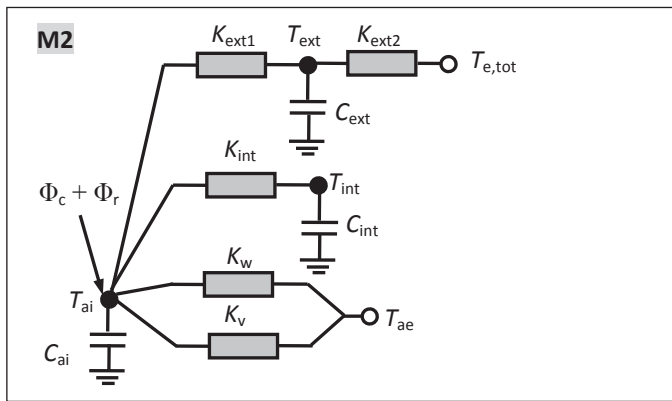


Fig. 2 The RC thermal circuit of model M2

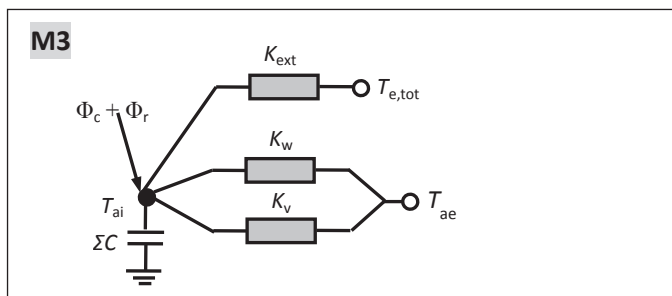


Fig. 3 The RC thermal circuit of model M3

thermal models can be understood as simplified resistance-capacitance (RC) thermal circuits reduced from complex thermal building models.

The identical model structure in model M2 was presented in Masy (2007). Kramer (2012) successfully used the almost identical model structure as model M2 to simulate historical buildings with significant thermal mass. Model M1 was probably first introduced in Tindale (1993). A one-node lumped parameter model similar to model M3 can be found in Burmeister and Keller (1998).

Thermal bridges

No lumped parameter models of thermal bridges have been found in literature. In principle, the following RC thermal circuits could be used to model different types of thermal bridges, see Figure 4.

Comments on model simplifications

Description of the internal environment

Model M1 decouples the radiative and convective heat transfer in the internal environment. There are two temperature nodes for the internal environment (the internal air temperature and the rad-air temperature). The coupling conductance K_x between the rad-air temperature node and the internal air temperature node is calculated as:

$$K_x = (\alpha_{ci} + \alpha_{ri}) \frac{\alpha_{ci}}{\alpha_{ri}} A \quad (1)$$

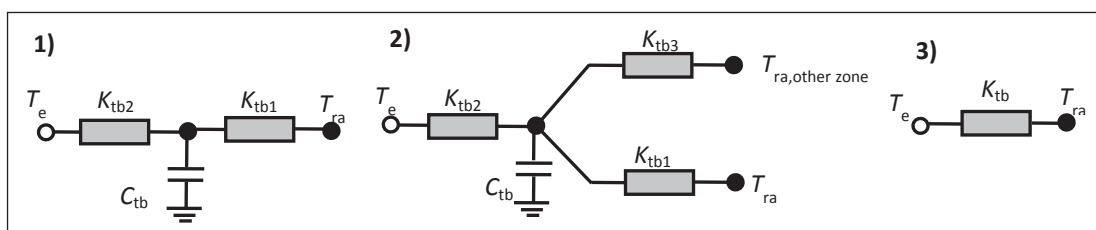


Fig. 4 Various RC thermal circuits for thermal bridges

where α_{ci} is the internal convective heat transfer coefficient, α_{ri} is the internal radiative heat transfer coefficient, and A_i is the area of the building components in contact with the internal air.

The way the concept of the two-node description of the internal environment has been derived and discussions on its validity are described in Davies (2004). Two temperature nodes for the internal environment are a mathematical product of series-parallel transformation where separate radiative and convective links with the surfaces are merged together. The internal surfaces of the building components are, thus, connected to the rad-air temperature by the combined surface thermal resistances. The coupling conductance K_x between the rad-air node and the internal air node and augmentation of the radiant heat gain do not have any physical interpretation.

Contrary to model M1, model M2 does not decouple the radiative and convective heat transfer (i.e., the internal environment is represented by one node). This corresponds to the very high value of the coupling conductance K_x in model M1. If the heat capacity of the thin mass layer in touch with internal surfaces is added to the value of C_{ai} , the central temperature T_{ai} in model M2 could be understood as the mean temperature composed of the internal air temperature, and the mean temperature of the thin mass layer close to the internal surface. Some error is, therefore, introduced into the ventilation heat flow. Moreover, some error is introduced into the thermostatic control, if the set-point is based on the internal air temperature.

Single-node representation of building components

The building components with significant thermal mass are represented by the one-node thermal networks in model M1 and M2. The one-node thermal network is used irrespective of the amount of material layers. Representation of a building component by a one-node thermal network can only be reasonable if the building component does not contain more than one layer with a significant thermal capacity. If an additional capacitive layer is located at the external surface (e.g., a veneer wall), a two-node model would be more appropriate.

Aggregation of parallel heat transfer paths

The thermal model of the external and internal building components in models M1 and M2 adopted two fundamental simplifying assumptions:

- ❑ The parallel heat transfer paths of the external building components were aggregated together.
- ❑ The parallel heat transfer paths of the internal building components were aggregated together.

Fraisse et al. (2002) analysed the aggregation of several heat transfer paths. He states that the aggregation of building components can only be reasonable if the thermal response of the building components in parallel to the boundary excitation is similar. This can be approximately true in many real-world cases (i.e., when a similar wall type or an internal partition is used within one building).

In some cases, either the internal or external building components may not contain significant amount of thermal mass, e.g., external

curtain walls or thin internal plasterboard partition walls. In this case, the structure of models M1 or M2 may be further reduced to second order models by omitting the corresponding thermal capacitance from the RC thermal networks.

The special case of model M2 (designated as M3) is introduced if the infinite value of the thermal conductance between the internal node and the capacity nodes is assumed (i.e., the temperature of thermal mass is in thermal equilibrium with the internal temperature), see Figure 3. The thermal mass in the building components is modelled using only one thermal capacitance which is immediately accessible for the purpose of storing heat gains.

Thermal excitation functions

Lumped parameter models are thermally excited both from the internal side of the building enclosure and from the exterior. For both sides, solar radiation plays an important role.

Solar heat gains through the windows are calculated by a separate model. The complexity of the solar heat gain model may differ. The calculated solar heat gains are then distributed between the internal air temperature node and the rad-air temperature node. Analogously, the internal heat gains (the metabolic heat of the occupants, the heat from electric appliances) and the heating or cooling power are split between both internal temperature nodes. The values of the convective/radiative split factors depend on, e.g., the amount of furniture in the case of solar heat gains, on the type of heating or cooling system, etc.

The heat exchange at the external surface of a building's components consists of the long-wave radiation exchange, particularly to the sky, the convective exchange, and the absorbed short-wave solar radiation. The net long-wave radiant surface-to-sky heat exchange cools the external surface, which is especially notable during clear windless nights. The short-wave radiation heats the external surface during the daytime. These three influences are mathematically expressed by the external equivalent temperature of a building component which can be calculated as:

$$T_e = \frac{\alpha_s G_{gt} + \alpha_{ce} T_{ae} + \alpha_{re} T_{re}}{\alpha_{ce} + \alpha_{re}} \quad (2)$$

where α_s is the short-wave absorptivity, α_{ce} is the convective heat transfer coefficient, α_{re} is the radiative heat transfer coefficient, and T_{re} is the mean radiant temperature of the surrounding surfaces. The long-wave radiation transfers heat between the external surface of a building component, the sky and the ground (the latter two surfaces are represented by the mean radiant temperature T_{re}).

The total external equivalent temperature $T_{e,tot}$ (i.e., the aggregated external temperature for the whole building) is calculated as the weighted mean from the thermal conductance of the individual external building components according to:

$$T_{e,tot} = \frac{1}{K_{ext}} \sum_{i=1}^m K_{ext,i} T_{e,i} \quad (3)$$

where K_{ext} is the total thermal conductance of the external building components and $K_{ext,i}$ is the thermal conductance of the i -th external building component. Equation (3) results from the equivalent thermal circuit where several parts of the parallel thermal conductance $K_{ext,i}$ were aggregated together. It is often reasonable to assume that total external equivalent temperature is equal to the temperature of the external air.

A simple white-box approach for estimating input parameters

The values of the input parameters in the lumped parameter models can be estimated in a forward manner from the available information about the buildings using standard and simple calculation procedures.

Building components

The thermal conductance K_{ext} and K_w are standard steady-state heat

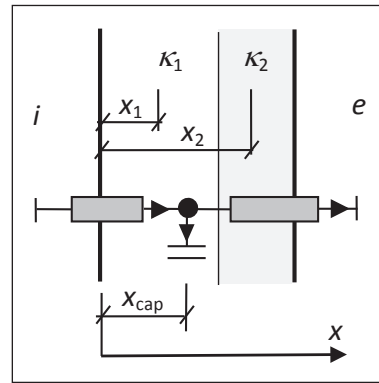


Fig. 5 The centre of the capacitance for a two-layer wall with a corresponding thermal circuit

transfer coefficients calculated from the thermal transmittance and corresponding heat exchange areas of the external building components ($K_{ext} = \sum U_i A_i$) and the windows, doors and any other fast heat transfer paths ($K_w = \sum U_{w,i} A_{w,i}$). The system of internal dimensions is used. The ventilation thermal conductance K_v is equal to the air flow rate multiplied by the volumetric heat capacity of air.

The thermal conductance K_{ext1} is calculated using the following procedure: At first, the total value of the thermal capacitance of the i -th external building component $C_{ext,i}$ is assumed to be located in the centre of the capacitance (see Figure 5).

The centre of the capacitance of the building components can be calculated as:

$$X_{cap} = \frac{\kappa_1 X_1 + \kappa_2 X_2}{\kappa_1 + \kappa_2} \quad (4)$$

where κ_1 (J/(m²K)) denotes the areal thermal capacity of layer 1, and κ_2 (J/(m²K)) denotes the areal thermal capacity of layer 2.

Based on the position of the centre of the capacitance, the values of the conductance $K_{ext1,i}$ for each external i -th building component are calculated. Finally, the thermal conductance $K_{ext1,i}$ are summed up to get the total lumped value of K_{ext1} . The same procedure is used for the calculation of the thermal conductance related to the internal building components K_{int} .

The thermal conductance K_{ext2} is then calculated from the relation:

$$\frac{1}{K_{ext}} = \frac{1}{K_{ext1}} + \frac{1}{K_{ext2}} \quad (5)$$

The total thermal capacitance of all the building component are summed up as well to get the total lumped values ($C_{ext} = \sum C_{ext,i}$, $C_{int} = \sum C_{int,i}$). The values of the thermal capacitance are not reduced in this study.

Thermal bridges

The thermal capacitance of the central node of a thermal bridge C_{tb} represents the thermal mass associated with intersections between the building components. Since the system of internal dimensions is used for calculations, the thermal mass in the intersections of the building components would be missing in the simulation models if not otherwise incorporated. The thermal conductance K_{tb} can be calculated from the estimated value of the linear thermal transmittance and the length of the corresponding thermal bridge ($K_{tb} = \Psi \times L$), respectively, from the point thermal transmittance and the number of point thermal bridges ($K_{tb} = X \times N_{tb}$).

COMPARISON WITH MEASURED DATA

Description of the experiment

Two side-by-side experiments were set up in the framework of the

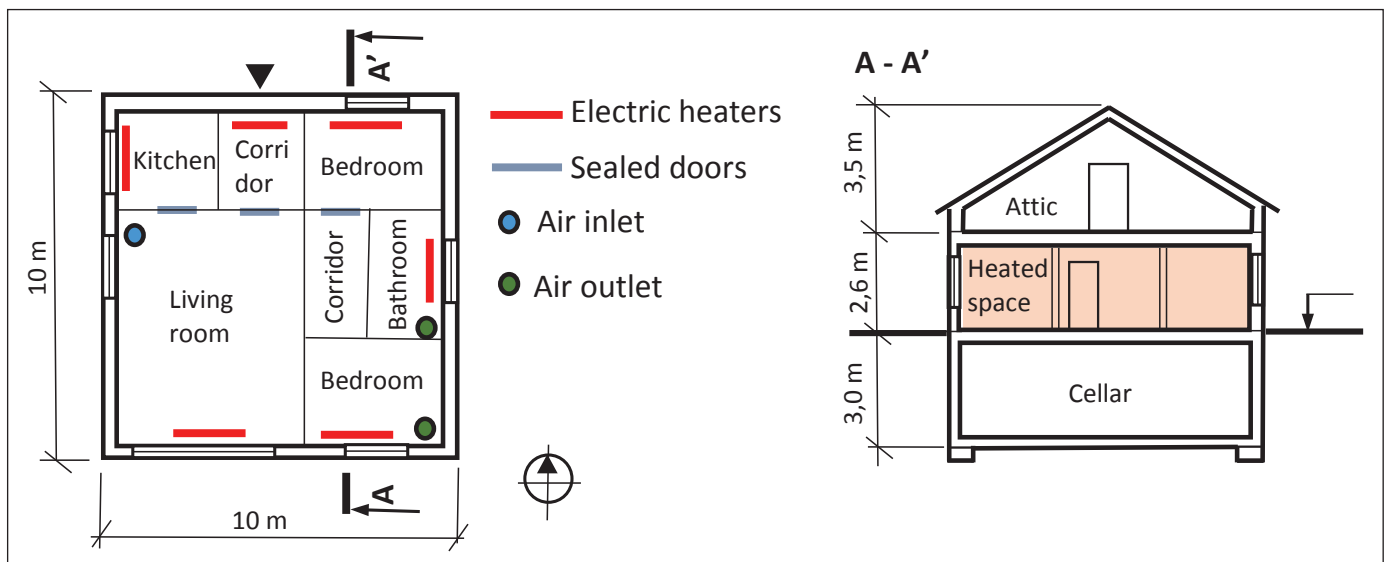


Fig. 6 Basic drawings of test family house

IEA Annex 58 “Reliable Building Energy Performance Characterisation Based on Full Scale Dynamic Measurements” with two identical family houses (designated as N2 and O5), see Figure 6.

The detailed specification of the experiments and measured data are accessible, see Strachan (2015). Kopecký and Staněk (2014) used the measured data in experiment 1 for comparison against the lumped parameter building models.

Experiment 1 consisted of consecutive periods of free-floating operation, random sequence for heat input (ROLBS) and a temperature-controlled operation (see Table 1 for the basic overview). There were no inhabitants in either house. Heating was ensured by conventional electrical heaters placed in front of the windows. The thermostatic control of the heaters was based on the measured air temperature at the mid-height of the room. The temperature in the attic, cellar and external environmental boundary conditions were monitored during the experiment.

Tab. 1 Time schedule of experiment 1

Period	Date	Description	Blinds on southern windows	
			House O5	House N2
P1	21.8.2013 – 29.8.2013	Initialisation, set-point 30 °C	Blinds up	Blinds down
P2	30.8.2013 – 13.9.2013	ROLBS in living room, no heat input in other rooms	Blinds up	
P3	14.9.2013 – 19.9.2013	Re-initialisation, set-point 25 °C	Blinds down	
P4	20.9.2013 – 30.9.2013	Free-floating	Blinds up	

For the purpose of modelling with the lumped parameter models, the house was divided in two zones. The south zone (zone 1, Z1) consisted of the living room, the internal corridor, the bedroom and the bathroom. The north zone (zone 2, Z2) consisted of the kitchen, corridor and bedroom. The north zone was not ventilated. The south zone was ventilated (a constant air flow rate of 120 m³/h). It was assumed that there was no air exchange between both zones (the doors were closed and sealed between both zones during the experiment, and had airtight building components between both zones).

The thermal zone was characterised by a measured mean internal air temperature and total heat input (see Figure 7). The mean internal air temperature of the zone was calculated from the measured data as a volume weighted average from the corresponding internal air temperatures.

Model details

The basic RC thermal circuits of the lumped parameter models (see Figure 1 to 3) were expanded in order to model the heat transfer through the floor (a thermal connection with the cellar), the heat transfer through the ceiling (a thermal connection with the attic) and the heat transfer through the dividing walls between both zones. These thermal paths in model M1 and model M2 were modelled by one-node RC thermal networks. The simplified model M3 used a single-conductance model for the above-mentioned building components. The doors between both zones were modelled by a single-conductance thermal network in all models.

Tab. 2 List of thermal bridges

No.	Description	Connected environments	Type of RC thermal circuit**	Ψ [W/(m·K)]	χ [W/K]
1	Ext. wall/Ext. wall	Int/Ext	1	0.09	-
2	Floor/Ext. wall	Int/Ext/Cellar	2	0.11	-
3	Ceiling/Ext. Wall	Int/Ext/Attic	2	0.085	-
4	Int. wall/Floor	Int/Cellar	1	0.38	-
5	Int. wall/Ceiling	Int/Attic	1	0.20	-
6	Partition/Floor	Int/Cellar	1	0.24	-
7	Partition/Ceiling	Int/Attic	1	0.13	-
8	Column/Floor	Int/Cellar	1	-	0.58
9	Column/Ceiling	Int/Attic	1	-	0.44
10	Window sill*	Int/Ext	3	0.03	-
11	Window lining*	Int/Ext	3	0.03	-
12	Window overhead*	Int/Ext	3	0.03	-

*Included in thermal conductance K_w

**See Figure 4 for thermal circuits.

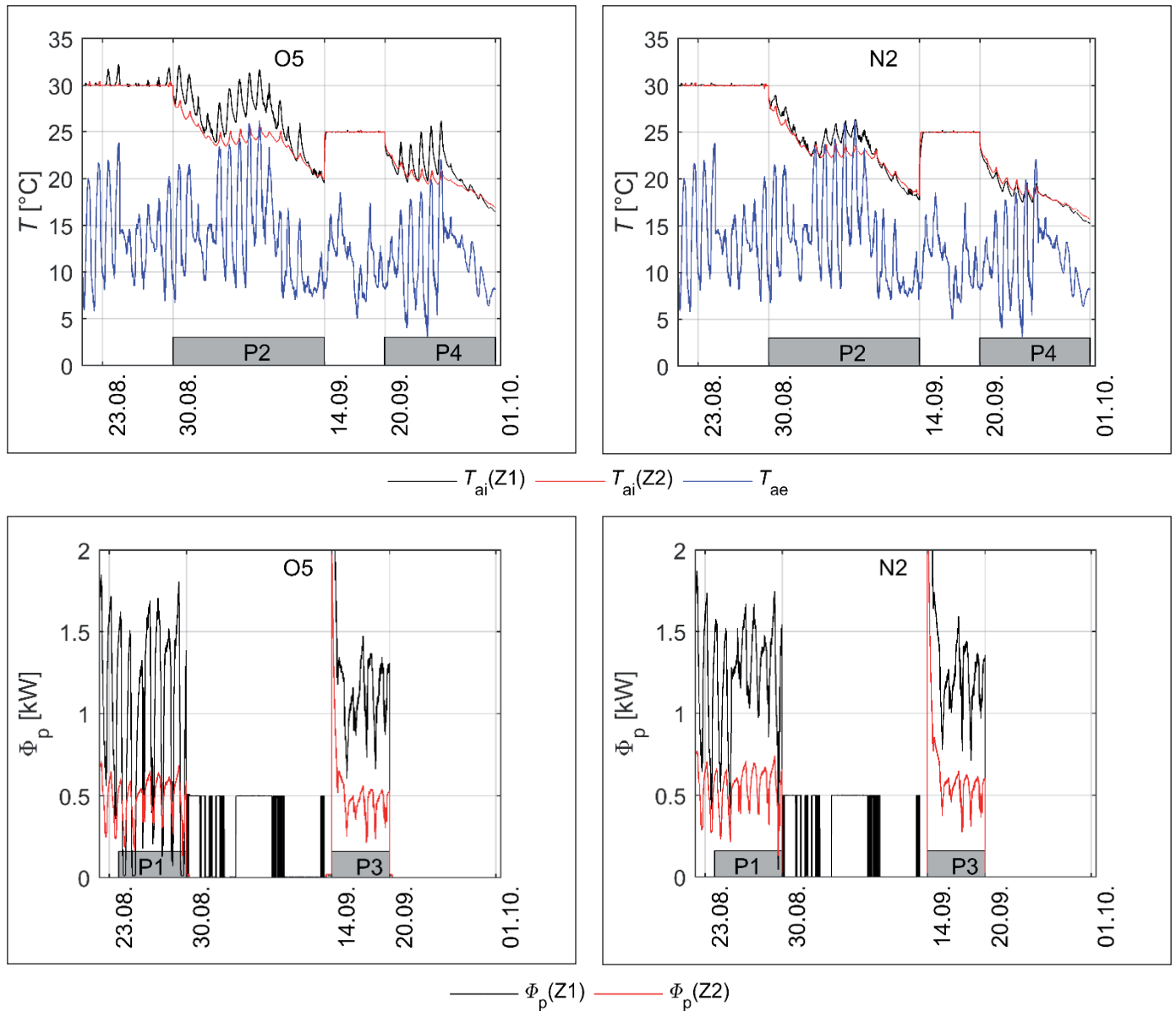


Fig. 7 The measured internal air temperature and the total heating power during experiment 1

The electric heaters were modelled as ideal heat sources with a negligible thermal capacity. The heat input from the convector heaters was distributed from 50 % to the air node, and from 50 % to the rad-air node.

The isotropic sky model was used to calculate the solar irradiance on a tilted oriented plane from the available solar irradiance on a horizontal plane. The solar energy transmittance of the glazing was treated as angular dependent. The solar heat gains were distributed from 90 % to the rad-air node, and from 10 % to the air node.

The list of thermal bridges is provided in Table 2. The values of the linear and point thermal transmittance were taken from the specification document.

Estimation of input parameters

The identical procedure as described in the previous text was used for the estimation of the input parameters. All material properties, component dimensions, and glazing properties, were consistently taken from the specification documents. The estimated input parameters in simplified parameter models are specified in Table 3.

The thermal conductance in the RC circuits of the thermal bridges were estimated from the total values of the thermal conductance K_{tb} . The thermal capacitance C_{tb} appearing in the RC circuits of the thermal bridges was estimated from the cross-sectional area of the thermal mass associated with the corresponding thermal bridge.

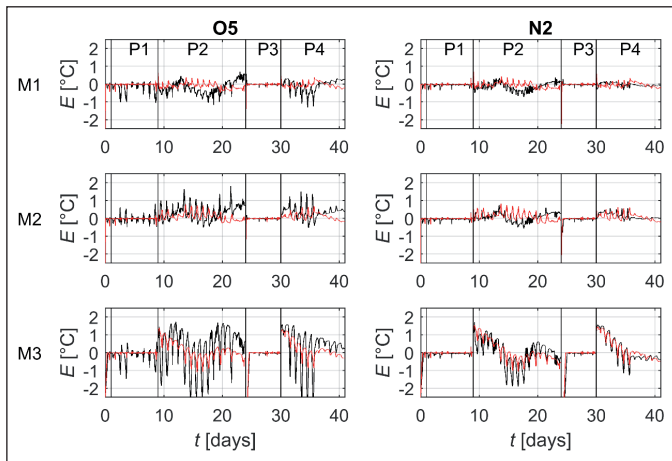
Tab. 3 The estimated values of the thermal parameters

Case	K_{ext} [W/K]	K_w [W/K]	K_v [W/K]	K_{ext1} [W/K]	K_{int} [W/K]	K_x^* [W/K]	C_{ext} [MJ/K]	C_{int} [MJ/K]	C_{ai}^{**} [MJ/K]	ΣC^{***} [MJ/K]
Z1	9.41	18.6	40.4	52.7	194.2	1079	12.6	5.63	1.79	28.4
Z2	7.68	8.77	0	39.2	96.5	552	9.74	2.84	1.70	18.1

*The coupling conductance K_x between the internal air temperature node and the rad-air temperature node was calculated with the assumption of: $\alpha_{ai} = 3 \text{ W}/(\text{m}^2\text{K})$, $\alpha_{ri} = 5 \text{ W}/(\text{m}^2\text{K})$, the total internal surface area $A_i = 224.8 \text{ m}^2$ (zone 1), resp. $A = 115.0 \text{ m}^2$ (zone 2).

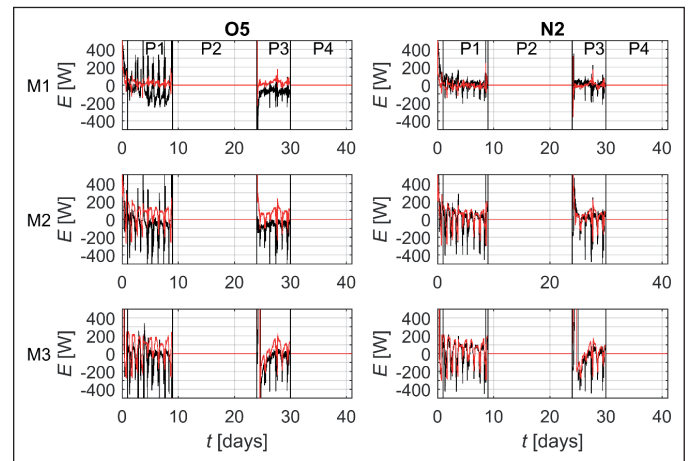
**The value of C_{ai} contains the thermal capacity of concrete columns and the thermal capacity of the internal window pane.

***The thermal capacity of the floor screed and half of the dividing walls was included.



— Z1 — Z2

Fig. 8 The simulation error of the internal air temperature (time profiles and histograms)



— Z1 — Z2

Fig. 9 The simulation error of the heating power (time profiles and histograms)

RESULTS AND DISCUSSION

The simulation was performed in an open loop mode with no feedback from the measured temperatures. The simulation error is defined as $E = \text{the calculated value} - \text{the measured value}$. The simulation errors (10-min averages) and the distribution of the simulation errors are depicted in Figure 8 and Figure 9. The mean errors (ME) of the heating power and internal air temperature are listed in Table 4. The relative errors (RE) of the delivered heat are listed in Table 5.

Generally, the simulation errors in house N2 are lower than the simulation errors in house O5. The simulation errors in both houses fluctuated with the daily period as they were correlated to the solar radiation. The daily oscillation of the simulation error was stronger in the unshaded house O5. Therefore, the inaccuracy is, to some extent, attributed with the quality of the solar heat gain calculation model. Moreover, the time profile of the simulation error of the internal air temperature contains the periodic component with a time period longer than one day. The long-term component of the simulation error is expected to be related to the number of temperature nodes in the models (coarse spatial resolution) and the inaccuracy of the solar heat gain calculation model.

Model M1 predicted the comparable shapes of the internal air temperatures and the heat inputs with the measured data. Model M1 exhibited the smallest error in the delivered heat (< 7 %), a small mean error in

Tab. 4 The mean error in the internal air temperature and heating power

House	Zone	Period	ME - T_{ai} [°C]			House	Zone	Period	ME - Φ_p [W]		
			M1	M2	M3				M1	M2	M3
O5	Z1	P2	-0.18	0.34	0.31	O5	Z1	P1	-36.4	-61.9	-86.4
		P4	-0.06	0.35	0.36			P3	-83.6	-87.4	22.2
	Z2	P2	-0.10	0.10	0.12		Z2	P1	18.6	54.4	65.6
		P4	-0.04	0.11	0.22			P3	30.7	71.2	130.7
Mean (abs(ME))			0.10	0.22	0.25	Mean (abs(ME))			42.3	68.7	76.2
N2	Z1	P2	-0.13	0.07	-0.02	N2	Z1	P1	6.4	-3.0	6.5
		P4	-0.03	0.13	0.15			P3	-4.5	-0.8	77.8
	Z2	P2	-0.07	0.10	0.09		Z2	P1	-7.2	27.1	35.8
		P4	-0.04	0.08	0.24			P3	2.7	51.6	114.5
Mean (abs(ME))			0.07	0.10	0.12	Mean (abs(ME))			5.2	20.6	58.7

the heating power (< 84 Watts) and a small mean error in the internal air temperature (0.18 °C). The error of model M1 has been mostly located within a bandwidth of ± 1 °C, i.e., the error was comparable with the uncertainty of the measured internal air temperature.

Tab. 5 The relative error of the delivered heat over the heating periods P1 and P3

House	Zone	Period	RE [-]		
			M1	M2	M3
05	Z1	P1	0.96	0.93	0.91
		P3	0.93	0.93	1.02
	Z2	P1	1.04	1.11	1.13
		P3	1.06	1.13	1.24
Mean(RE)			1.00	1.03	1.08
N2	Z1	P1	1.01	1.00	1.01
		P3	1.00	1.00	1.06
	Z2	P1	0.99	1.05	1.07
		P3	1.00	1.08	1.17
Mean(RE)			1.00	1.03	1.07

Model M3 achieved the worst match with the measured data. The time profile of the heating power was not accurately predicted. The shape of the internal air temperature was not accurate as well. The daily swing of the internal air temperature was attenuated too much and the daily peak culminated too late. However, the mean error in the heating power, the mean error in the internal air temperature and the delivered heat were close to the measured values of the experiment.

Model M2 achieved better agreement with the measured data than model M3. The time profile of the internal air temperature was very similar to the measured profile. The mean error in the heating power was higher than in the case of model M1. The shape of the heating power was not predicted as good as in the case of model M1. The simulation errors of model M2 were distributed in a wider interval than in model M1.

Model M1 distributed the heat between the internal air temperature node and the rad-air temperature node. This feature probably better represents the physical reality. However, it also imposes uncertainty of the real values of the convective/radiative split for the solar heat gains and the heat emitted by the heating system. In fact, the time profile of the heating power in the experiment was rather sensitive to the setting of the heat distribution from the electric heating bodies.

The compensation of the errors is the principal problem of the validation. The similar internal air temperature profiles may be generated by different input parameter setups. For instance, heat gains and heat losses could be simultaneously overestimated or underestimated. Both combinations would lead to similar model outputs. Moreover, if a modeller gets an impression that heat losses have been probably underestimated it is difficult to distinguish whether the heat transfer path is inaccurately modelled (i.e., the model is too coarse) or is there is an inadequate setting of the input parameters.

CONCLUSIONS

This paper assessed three selected lumped parameter building thermal models. The simplifying assumptions and a simple method for the estimation of the input data have been discussed and described. We identified the third order lumped parameter thermal model as being capable of predicting the dynamic thermal performance of a real scale test buildings. The third order model could, therefore, be used as an initial

choice if the objective is to implement a model predictive controller in a building. In reality, some additional temperature nodes might be needed to be added in the basic thermal circuit, e.g., if the heating and cooling system are integrated in the thermal mass.

Contact: pavel.kopecky@fsv.cvut.cz

Acknowledgement. This work has been supported by the Ministry of Education, Youth and Sports within the National Sustainability Programme I (NPU I), project No. LO1605 – University Centre for Energy Efficient Buildings – Sustainability Phase.

Symbols:

- A_i Area of the building components in contact with the internal air [m²]
- C_{ai} Thermal capacitance of the internal air [J/K]
- C_{ext} Total thermal capacitance of the external building components [J/K]
- C_{int} Total thermal capacitance of the internal building components [J/K]
- C_{tb} Thermal capacitance of a thermal bridge [J/K]
- G_{gt} Global solar irradiance on a tilted oriented plane [W/m²]
- K_{ext} Total thermal conductance of the external building components [W/K]
- K_{ext1} Total thermal conductance between the internal environment and the aggregated external building components [W/K]
- K_{int} Total thermal conductance between the internal environment and the aggregated internal building components [W/K]
- K_w Total thermal conductance of the windows [W/K]
- K_v Thermal conductance due to ventilation [W/K]
- K_x Coupling conductance between the internal air node and rad-air node [W/K]
- T_{ai} Internal air temperature [°C]
- T_{ae} External air temperature [°C]
- T_{ra} Rad-air temperature [°C]
- T_{ext} Mean temperature of the external building components [°C]
- T_{int} Mean temperature of the internal building components [°C]
- T_{tb} Mean temperature of a thermal bridge [°C]
- T_e External equivalent temperature (sol-air temperature) [°C]
- Φ_r Radiant part of the heat gains [W]
- Φ_c Convective part of the heat gains [W]
- Φ_p Heating or cooling power [W]
- α_c Convective heat transfer coefficient [W/(m²K)]
- α_r Radiative heat transfer coefficient [W/(m²K)]
- α_s Absorptivity of the short-wave radiation (solar absorptivity) [-]

Lower indexes

- ext External building components (thermal connection to the exterior)
- int Internal building components (no thermal connection to the exterior)
- V Ventilation
- inf Infiltration
- w Windows
- i Internal
- e External
- a Air
- c Convection or cooling
- r Radiation
- ae Air, external
- ai Air, internal
- tb Thermal bridges

References

- [1] TOKE, RAMMER, NIELSEN. Simple tool to evaluate energy demand and indoor environment in the early stages of building design. *Solar Energy*. 2005, vol. 78, issue 1, pp. 73-83. ISSN 0038-092X. <https://doi.org/10.1016/j.solener.2004.06.016>.
- [2] REYNDERS, G., NUYTEN, T., SAELENS, D. Potential of structural thermal mass for demand-side management in dwellings. *Building and Environment*. 2013, vol. 64, pp 187-199. ISSN 0360-1323. <https://doi.org/10.1016/j.buildenv.2013.03.010>.

- [3] KÄMPF, J., H., ROBINSON, D. A simplified thermal model to support analysis of urban resource flows. *Energy and Buildings*. 2007, vol. 39, issue 4, pp. 445-453. ISSN 0378-7788. <https://doi.org/10.1016/j.enbuild.2006.09.002>.
- [4] HUIJBREGTS, Z., KRAMER, R.P., MARTENS, M.H.J. van SCHIJNDEL, A.W.M., SCHELLEN, H.L. A proposed method to assess the damage risk of future climate change to museum objects in historic buildings. *Building and Environment*. 2012, vol. 55, pp. 43-56. ISSN 0360-1323. <https://doi.org/10.1016/j.buildenv.2012.01.008>.
- [5] KRAMER, R., van SCHIJNDEL, J., SCHELLEN, H. Simplified thermal and hygric building models: A literature review. *Frontiers of Architectural Research*. 2012, vol. 1, issue 4, pp. 318-325. ISSN 2095-2635. <https://doi.org/10.1016/j.foar.2012.09.001>.
- [6] BURMEISTER, H., KELLER, B. Climate surfaces: a quantitative building-specific representation of climate. *Energy and Buildings*. 1998, vol. 28, issue 2, pp. 167-177. ISSN 0378-7788. [https://doi.org/10.1016/S0378-7788\(98\)00012-7](https://doi.org/10.1016/S0378-7788(98)00012-7).
- [7] TINDALE, A. Third-order lumped-parameter simulation method. *Building Service Engineering Research Technology*. 1993, vol. 14, issue 3, pp. 87-97. <https://doi.org/10.1177/014362449301400302>.
- [8] MASY, G. *Definition and Validation of a Simplified Multizone Dynamic Building Model Connected to Heating System and HVAC Unit*. PhD Thesis. Université de Liège, 2007. Available at: <http://bictel.ulg.ac.be/ETD-db/collection/available/ULgetd-11052008-145605/>
- [9] DAVIES, M., G. *Building Heat Transfer*. Wiley, 2004.
- [10] PRÍVARA, S., ŠIROKÝ, J., FERKL, L., CIGLER, J. Model predictive control of a building heating system: The first experience. *Energy and Buildings*. 2011, vol. 43, issues 2-3, pp. 564-572. ISSN 0378-7788. <https://doi.org/10.1016/j.enbuild.2010.10.022>.
- [11] JUDKOFF, R., NEYMARK, J., *International Energy Agency Building Energy Simulation Test (BESTEST) and Diagnostic Method*. NREL, 1995.
- [12] MATHEWS, E.H., RICHARDS, P.G., LOMBARD, C. A first-order thermal model for building design. *Energy and Buildings*. 1994, vol. 21, issue 2, pp. 133-145. ISSN 0378-7788. [https://doi.org/10.1016/0378-7788\(94\)90006-X](https://doi.org/10.1016/0378-7788(94)90006-X).
- [13] FRAISSE, G., VIARDOT, CH., LAFABRIE, O., ACHARD, G. Development of a simplified and accurate building model based on electrical analogy. *Energy and Buildings*. 2002, vol. 34, issue 10, pp. 1017-1031. ISSN 0378-7788. [https://doi.org/10.1016/S0378-7788\(02\)00019-1](https://doi.org/10.1016/S0378-7788(02)00019-1).
- [14] STRACHAN, P. *Twin Houses Empirical Dataset: Experiment 1*. University of Strathclyde. *Empirical_Modelling_Specification_200514*(.pdf), *Supplementary_files*(.zip), *Supplementary_file_structure*(.txt). 10.15129/8a86bbbb-7be8-4a87-be76-0372985ea228